1 # **Numerical Simulation of Wind Drift of Arrows on the**
2 # **Olympic Venue for Tokyo 2020**
3

4 *In the present work, the dynamics of archery arrows is studied by means of a*
5 *mathematical model to evaluate their response to different wind characteristics and*
6 *initial conditions. Numerical computations are performed to quantify the effect that*
7 *the background wind has on the dynamics of the arrows during their flights.*
8 *Aerodynamic and physical characteristics of two commercial arrows are considered.*
9 *The background wind information from the venue where the Archery competition will*
10 *be held in the Tokyo Olympic Games in 2020 was provided by JAMSTEC. In a*
11 *simulated archery range of 70 m, the heavier arrow showed a lateral deviation from*
12 *the center of the target of ~0.11 m, whereas the lighter arrow showed a final deviation*
13 *in its trajectory of ~ 0.15 m. The ratio of the drag force to the gravitational force plays*
14 *a key role in determining the deviation in the trajectory. By keeping the boundary*
15 *layer laminar, a less deviated shot can be achieved. With increasing arrow's initial*
16 *velocity, the deviation in the trajectory also reduces.*
17

20

21

22 ## **Introduction**
23

24   In this paper the effect of different types of background winds in the
25 dynamics of archery arrows by means of numerical simulations is studied.
26 Archery competition is a sports discipline in which the accuracy and precision
27 are key factors in order to obtain a good final score. In the competitions using a
28 recurve bow, the archers aim at a target with 1.22 m in diameter and located 70
29 m away. The target is divided into 10 smaller evenly spaced concentric circles,
30 rings. The innermost of the rings has a diameter of 0.122 m and is assigned
31 with the maximum of 10 points. The archers shoot a specified number of
32 arrows and the one who sums more points wins the competition. Striking the
33 innermost ring gives the opportunity to elevate the final score, which is
34 complicated if the multiple elements affecting the shots are considered.
35   In recent years, the sports engineering became a flourishing research field
36 for engineers due to the realization of the positive impact of using modern
37 tools and techniques in the design and testing stages of sports equipment. The
38 literature covers a wide range of examples [Allen T, 2017] for various sports
39 and approaches, including pole vault [Haake S, 2009] and sport projectiles
40 [Goff J, 2013 and Kooi B, 1998], water channel experiments [Park et al., 2011]
41 and computational techniques [Hubbard M, 1984 and Park L, 2011]. It is
42 expected that an adequate design and technology selection may reduce errors
43 and improve the performance in the competitions. The latter represents the
44 motivation for our group to carry out a detailed study of archery arrows, in
45 order to understand their dynamics and clarify some of the effects that take
46 place during the competitions.

1   An important factor that cannot be controlled by the archers is the
2 background wind, and we can refer to it as one of the most important elements
3 disturbing the shots. Recently, Park [Park, 2019] reported a detailed compiling
4 of some of the last published works related with the effect of the atmosphere
5 conditions in the performance in the archery shots.

6   In the present work is analyzed the external ballistics of the arrows, i.e.
7 their behavior while flying in their way to the target when the background
8 wind exerts its influence. Ballistics is a well-studied area in physics,
9 nevertheless the dynamics of archery arrows still of interest due to their
10 complex behavior during free-flight. An arrow translates, rotates and oscillates
11 longitudinally around its center of mass while flying, making complex the
12 analysis of the aerodynamic forces exerted on it. Also, the flight of arrows shot
13 with a recurve bow last less than 1.5 s in the air with an initial velocity of
14 around 57 ms^{-1}.

15   In a previous work of our group, there were measured some of the physical
16 and aerodynamic characteristics of two commercial arrows [Ortiz et al., 2019]
17 and then by using such properties the arrows' trajectory and attitude were
18 computed. Arrows with larger mass showed less sideward deviation in their
19 trajectories, wind drift, independently of the wind velocity. The wind was
20 considered to show two different behaviors. For the first case, uniform type
21 winds were simulated, in which the wind velocity remains constant regardless
22 the position of the arrow during free-flight. In the second one, the wind showed
23 a sinusoidal-type evolution along the archery range, with a maximum wind
24 velocity of 3 ms^{-1} at the middle of the track. Under the influence of the former
25 type of wind with 3 ms^{-1}, the radial deviations from the center of the target
26 were computed to be 0.34 m and 0.26 m for the lighter and heavier arrows,
27 respectively.

28   Nevertheless, the two previously described winds might be unusual.
29 During a real outdoors competition, is expected that winds along the archery
30 range change spatially and temporary. The velocity and direction of the wind
31 might vary abruptly, adding difficulty to the shots and provoking an
32 unexpected arrows' behavior. The present work takes into account the wind
33 characteristics where the archery competition will be held in the Tokyo
34 Olympic Games in 2020. The wind information was computed using a Large
35 Eddy Simulator (LES), developed by the Japan Agency for Marine-Earth
36 Science and Technology (JAMSTEC). The main characteristic of the wind
37 behavior information provided by JAMSTEC is that the wind component
38 velocities vary with time and position, allowing to test the response of
39 commercial arrows under a realistic environment.

40   In this work, we investigate the influence of the mass, initial velocity and
41 initial angular velocity in the dynamics of the archery arrows. Also, the
42 behavior of the arrows under uniform and changing winds is compared.
43 Finally, the influence of the delay in the transition of the arrow's boundary
44 layer is studied.

45   This work is organized as follows, in the section "General Characteristics"
46 are provided the descriptions of the arrows, mathematical model, background

wind and initial conditions. In the section "Results" we show the findings from the numerical computations. In the section "Discussions" are studied the cases for which exist a delay in the transition of the boundary layer. In the section "Conclusions" we make the last comments with a brief summary.

General Characteristics

Description of the arrows

Archery arrows are composed of an elongated shaft, a point located at its front, a set of vanes and a nock at its rear part. In this study, the physical and aerodynamic characteristics of two commercial arrows, obtained in previous experiments of our group [Ortiz et al., 2019], are considered. Both studied arrows are manufactured from an aluminum alloy tube with an external carbon sheet as cover. We refer to them as the type-A and type-B arrows.

The physical characteristics mass (M), radius (r), length (l), moments of inertia around the axis perpendicular to $\boldsymbol{n}$ (I) and around $\boldsymbol{n}$ (I_3), respectively, are listed in Table 1. The aerodynamic characteristics are listed in Table 2. The parameters α and β are related with the lift and pitching moment, respectively. Also, the spin parameter (S_P) and the initial velocity of the arrows (V_0) are shown. Two different values of the drag coefficients for the laminar, C_D (lam), and turbulent, C_D (turb), regimes are taken into account in the simulations. The former is used when the ideal initial angular velocity is achieved (see the section "Initial conditions"). Whereas the latter is used when such ideal initial conditions cannot be achieved. The archery arrows are light and flexible, nevertheless the difference of ~0.005 kg in mass play an important role in their dynamics.

Table 1. *Physical Characteristics of the Arrows*

Symbol	Name	Type-A	Type-B
r [m]	Radius	2.62×10^{-3}	2.40×10^{-3}
l [m]	Length	0.625	0.625
M [kg]	Mass	0.0142	0.0197
I [kgm^2]	Moment of inertia	6.98×10^{-4}	8.97×10^{-4}
I_3 [kgm^2]	Moment of inertia	2.81×10^{-7}	3.23×10^{-7}

Table 2 *Aerodynamic Characteristics of the Arrows*

Symbol	Name	Type-A	Type-B
α [1/rad]	Parameter alpha	40.2	45.1
β [1/rad]	Parameter beta	16.2	21.2
S_P	Spin parameter	0.029	0.034
C_D (lam)	Drag coefficient	1.50	1.63
C_D (turb)	Drag coefficient	2.69	3.23

V_0 [ms^{-1}]	Initial velocity	57.3	56.7

3

4   For comparison, we refer to another sports where the dynamics of the
5 projectiles plays a key role, say the javelin throw. Even though archery and
6 javelin throw differ in many aspects, the javelins are subject to the same
7 aerodynamic forces as the archery arrows and serve us to remark some
8 important physical characteristics. Javelins are long spears with a mass of
9 around 0.80 kg and a fineness ratio $f = 80$. The initial launching velocity for
10 javelins is about 30 ms^{-1}. While studying the dynamics of flying javelins,
11 Hubbard [Hubbard, 1984] found that these projectiles develop large angles of
12 attack during their flight ($\gamma_{max} > 35°$) leading to large lift forces necessary to
13 increase the range that would make the thrower to get a high score in the
14 competition. Such values of γ also induce a large drag component that leads to
15 less precise shots. In javelin throw, precision is not as relevant as in the archery
16 competition.
17   One important difference between the aerodynamics of arrows and
18 javelins is the position of their corresponding center of pressure *c.p.* and center
19 of gravity *c.g.* In javelins, *c.p.* is found very close to *c.g.,* at around 8×10^{-3} m
20 [Hubbard, 1984]. Whereas in the case of the arrows, *c.g.* is located in the front
21 part while *c.p.* in the tail, having a distance of around 0.40 m between them.
22 The fact that *c.p.* and *c.g.* are very close represents an absence of pitching
23 moment in the javelin's flight. Therefore, no counterbalance effect to the
24 increasing angle of attack takes place. The growing magnitude of γ allows to
25 generate large values of lift and drag forces. Contrary, the maximum value of
26 the angle of attack computed by Miyazaki et al. [Miyazaki et al., 2017] in
27 arrows in free flight, under still air conditions, is around $\gamma_{max}=0.4°$. This small
28 angle of attack is a product of the pitching moment-lift force balance effect.
29 Such small γ generates smaller drag force and drift in an arrow than in a javelin,
30 allowing precise shots.

31

32 *Description of the Mathematical Model*

33

34   In this study, the equations of a rigid body simulating an archery arrow are
35 computed. Such model disregards the flexural oscillation of the real arrows in
36 free-flight, which simplifies the study of these projectiles. We define a fixed
37 coordinate system *x*, *y* and *z* with the corresponding unit vectors *i, j* and *k*, as
38 shown in Fig.1. Besides the gravitational force (g), exerted on the vertical
39 direction (z), the movement of the arrow is influenced by the background wind,
40 which is $U= (u_x, u_y, u_z)$. In the defined coordinate system, *x* and *y* form a
41 horizontal plane or the ground. The velocity of the arrow's center of mass is $V=$
42 ($V\sin\Theta \cos\Phi$, $V\sin\Theta \sin\Phi$, $V\cos\Theta$). Two unit vectors, $t = V–U/ | V–U |$ and $n=$
43 ($\sin\theta \cos\phi$, $\sin\theta \sin\phi$, $\cos\theta$) are considered. The former along the vector sum of
44 the relative velocity of the arrow's center of mass and the wind, $V–U$. Whereas
45 the latter along the arrow's axis, as shown in Fig.1. Consider θ and Θ as the

angles formed between n and t with z, respectively. Whereas ϕ and Φ are measured between the ground projection of n and t with x, respectively.

As the arrow translates in free-flight, a misalignment between n and t is expected due to the background wind influence. Such misalignment is characterized as the angle of attack $\gamma = \cos^{-1}[n \cdot t]$. The computation of the time evolution of γ is of interest due to from its value can be inferred the state of the boundary layer [Ortiz et al., 2019].

The aerodynamic loads drag (F_D) and lift (F_L) must be considered during the flight simulation. These forces are exerted contrarily and perpendicularly to $V - U$, respectively. The drag and lift forces are,

$$F_D = -\frac{1}{2}C_D\rho\pi r^2|V - U|(V - U),\tag{1}$$

$$F_L = \frac{1}{2}\alpha\rho\pi r^2[|V - U|^2n - n \cdot (V - U)(V - U)],\tag{2}$$

respectively. Where C_D is the drag coefficient and ρ is the air's density. The parameter α is related to the lift coefficient with $C_L = \alpha\gamma$ and is determined experimentally [Ortiz et al., 2019]. The arrow's radius is r.

The angular momentum is $L = In \times dn/dt + I_3\omega_3 n$, where I and I_3 represent the moments of inertia around the axis perpendicular to n and around it, respectively. ω_3 is the axial angular velocity component. Therefore, the equations of motion are expressed as

$$M\frac{dV}{dt} = -Mg k + F_D + F_L,\tag{3}$$

$$\frac{dL}{dt} = In \times \frac{d^2n}{dt^2} + I_3\left(\frac{d\omega_3}{dt}n + \omega_3\frac{dn}{dt}\right)$$

$$= \frac{1}{2}\beta\rho\pi r^2 l|V - U|n \times (V - U) + N_3 n,\tag{4}$$

Figure 1. *Illustration of an Arrow in Free-Flight with the Relevant Variables Considered in the Mathematical Model*
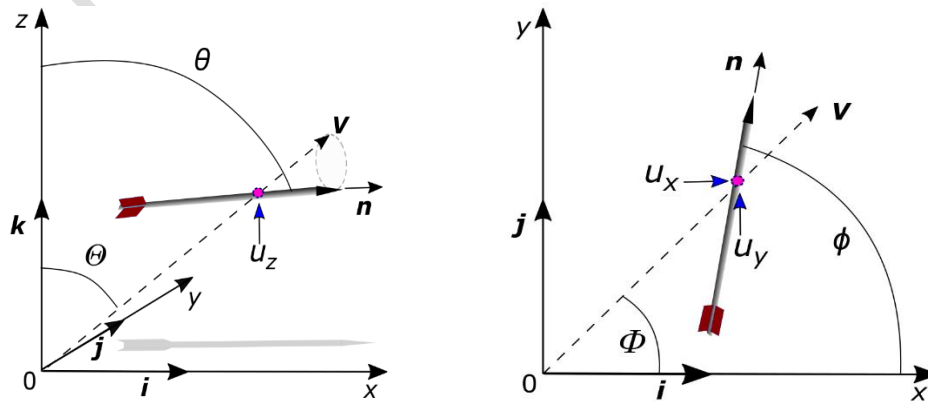
1

2   **(a)**   **(b)**

3 *Source*: Authors.

4

5 where M is the arrow's mass, g is the gravitational acceleration and N_3 is

6 the axial component of the torque. The parameter β is related with the pitching

7 moment coefficient by $C_M = -\beta\gamma$ and it is determined experimentally [Ortiz et al.,

8 2019]. Since we do not have any information about N_3 and then the time

9 evolution of the angular velocity is unknown, is necessary to approximate its

10 value assuming that $S_P = \omega_3 r/|V - U|$ is constant [Miyazaki et al., 2012 and

11 Miyazaki et al., 2017]. Here, S_P is the spin parameter, which is obtained from

12 wind tunnel experiments. This assumption is valid for small angles of attack, $|\gamma|$

13 $< 3.0°$.

14   To solve such a system composed by Eqs. (3-4), it is necessary to compute

15 dV/dt, $d\Theta/dt$, $d\Phi/dt$, $d\omega_\theta/dt$ and $d\omega_\phi/dt$, where $d\theta/dt = \omega_\theta$ and $d\phi/dt = \omega_\phi$. The

16 system is solved by using a standard 4th order Runge-Kutta method with a

17 time step $\Delta t = 5 \times 10^{-4}$ s.

18

19 *Description of the Simulated Archery Range*

20

21   The venue for the archery competitions in the Tokyo Olympic Games

22 2020 will be held in the semi-closed bay of Tokyo in Yumenoshima Park, Fig.

23 2. The area is located to the east of Tokyo Metropolitan area near to the sea and

24 has a surface of ~95,000 m^2. At the moment of writing, the main venue

25 location has been decided but the final design of the archery stadium(s) and

26 facilities are not available for the public yet. Therefore, we project the

27 existence of two possible main competition areas inside the sporting complex.

28 We refer to them as the *final round area* (fields I, II and III), at the western part

29 of the complex, and the *ranking round area* (fields IV, V and VI), Fig. 3. Each

30 of the tracks are north oriented with a shooting direction south-north and are

31 simulated to have a dimension of 70 m × 5 m. At 70 m from the shooting

32 position, it is located a target that has 1.22 m in diameter. It is recognized that

33 the presence of buildings and the local plant canopy affect

34

1

2 **Figure 2.** *Yumenoshima Park in the bay of Tokyo, where the Archery*
3 *Competitions will be held in the Olympic Games in Tokyo 2020.*

4
5 *Source*: Authors.

6

7 **Figure 3.** *Illustration of the Considered Archery Ranges, the Fields I-III are*
8 *Considered as the Final Round Area. Whereas the Fields IV-VI are the*
9 *Ranking Round Area.*

10
11 *Source*: Authors.

1

2   seriously the wind patterns [Neda and Rajat, 2018], which must be taken

3   in consideration in future studies.

4   Due to the wind effect, the arrows are expected to show deviations in the

5   trajectory, which can be measured at 70 m using their striking points with the

6   target. Such deviations from the center of the target are δy and δz in the y and z

7   directions, respectively. The radial deviation from the center of the target is

8    $\delta r = (\delta y^2 + \delta z^2)^{1/2}$. Such deviations are measured and compared for the different

9   types of winds and initial conditions.

10   The data corresponding to the time depending wind information in the

11   venue was obtained by means of the high-resolution numerical simulations'

12   results and provided by JAMSTEC. To compute the wind components, they

13   used the Multi-scale Simulator for the Geoenvironment (MSSG) model

14   [Matsuda et al., 2018]. The MSSG is an atmosphere-ocean coupled general

15   circulation model that, at urban scales, may work as a large-eddy simulator

16   (LES) with the capability to include local building shapes. The simulated wind

17   data describes a typical clear day of August 2007 in the Tokyo bay with sea

18   breeze. This information corresponds to a plane located at 2.5 m from the

19   ground with a horizontal resolution of 5 m. The wind velocity components

20   change with the position and time during 30 s with a time step of 0.1 s. In Fig.

21   2 and Fig. 3, the original satellite images were obtained from Google Earth Pro

22   and correspond to the current state of the field in October 2018.

23

24   *Computation of the Background Wind at any Instant and Position*

25

26   Because JAMSTEC provides three wind components on a plane at 2.5 m

27   from the ground level with a horizontal resolution of 5 m, it is necessary to

28   inter- and extrapolate the wind information at any arrow's position and time.

29   The surface layer approach is used to obtain the wind (u_x u_y and u_z) that the

30   arrow experiences along its free-flight. The vertically logarithmic wind profile

31   can be described with $u_x = u_{x*}/k \ln (z/z_{\mathrm{rl}})$ and $u_y = u_{y*}/k \ln (z/z_{\mathrm{rl}})$. Here,

32   k is the universal von Karman's constant and has an experimentally determined

33   value of $k \approx 0.4$. The value of z is the position of the arrow's center of mass

34   with respect to the ground and z_{rl} corresponds to the roughness length, whose

35   typical value for a grassy field is $z_{\mathrm{rl}}=0.01$ m. The friction velocities u_{x*} and u_{y*}

36   are computed for each iteration with

37

38
$$u_{x\,(2.5)} = \frac{u_{x*}}{k}\ln\left(\frac{2.5}{z_{\mathrm{rl}}}\right), \tag{5}$$

39

40
$$u_{y\,(2.5)} = \frac{u_{y*}}{k}\ln\left(\frac{2.5}{z_{\mathrm{rl}}}\right), \tag{6}$$

41

42   where $u_{x\,(2.5)}$ and $u_{y\,(2.5)}$ are the x and y components of the wind at 2.5 m

43   from the ground level and provided by JAMSTEC. Therefore, the wind

44   velocities in the x and y directions at any instant and location are obtained with

45

1 $$u_x = \frac{u_{x\,(2.5)} \ln\left(\frac{z}{z_{rl}}\right)}{\ln\left(\frac{2.5}{z_{rl}}\right)}, \qquad\qquad (7)$$

2

3 $$u_y = \frac{u_{y\,(2.5)} \ln\left(\frac{z}{z_{rl}}\right)}{\ln\left(\frac{2.5}{z_{rl}}\right)}. \qquad\qquad (8)$$

4

5 If the condition of continuity is considered, $\nabla \cdot U = 0$, the vertical component of
6 the wind, u_z, can be obtained by using

7

8 $$u_z = 0.0884\, u_{z(2.5)} \left[z \ln\left(\frac{z}{z_{rl}}\right) - z + 0.01 \right], \qquad\qquad (9)$$

9

10 where $u_{z\,(2.5)}$ is the known vertical wind velocity at 2.5 m. The solution of Eqs.
11 (3-4) allows to know the position, x_i, y_i and z_i, of the arrow's center of mass at
12 any instant, t_i. Whereas by solving Eqs. (7-9), it is possible to obtain the wind
13 components u_{xi}, u_{yi} and u_{zi} for such position. Nevertheless, the change in the
14 arrow's center of mass location is computed in orders of mm ($O\,(10^{-3})$),
15 whereas the spatial resolution of the wind information is 5 m. Therefore, the
16 wind components at any arrow's position were spatially interpolated. Further,
17 the time interval for the wind data provided by JAMSTEC is 0.1 s, whereas the
18 time step in the Runge-Kutta computation is 5×10^{-4} s, resulting necessary to
19 perform a time interpolation of the wind components at each time step. For
20 both the spatial and time interpolations, a cubic spline method was used.
21 Fig.4 shows the time evolution of the velocity for the three wind components
22 along the total length of the fields II and V at a distance $z = 2.5$ m from the
23 ground during 30 s. The wind velocity ranges from -1 ms^{-1} to 3.5 ms^{-1}. In
24 Figs.4a-4b, the predominance of south-north (tail-winds, $u_x > 0$) wind currents is
25 appreciated in both fields due to the presence of the ocean at the south of the
26 archery venue. In the field II at ~30 m, from the shooting position (Fig.4a) and
27 $t_0 = 0$ s, the tail-winds show a maximum velocity of $u_x \sim 3.2$ ms^{-1} and reduces
28 gradually until $u_x \sim 0.25$ ms^{-1}.
29   Regarding to the side-wind component in the field II (Fig. 4c), there exists
30 predominance of positive side-winds ($u_y > 0$) whereas in the field V the side-
31 wind velocity remains negative ($u_y < 0$) during most of the time (Fig. 4c). The
32 vertical wind component in Figs. 4e and 4f is negative along both tracks, $u_z <$
33 0. As appreciated from the Fig.4, the wind conditions change with the position
34 and the time. Such kind of behavior might be expected in archery ranges
35 located outdoors. The archer's lack of knowledge of the wind behavior may
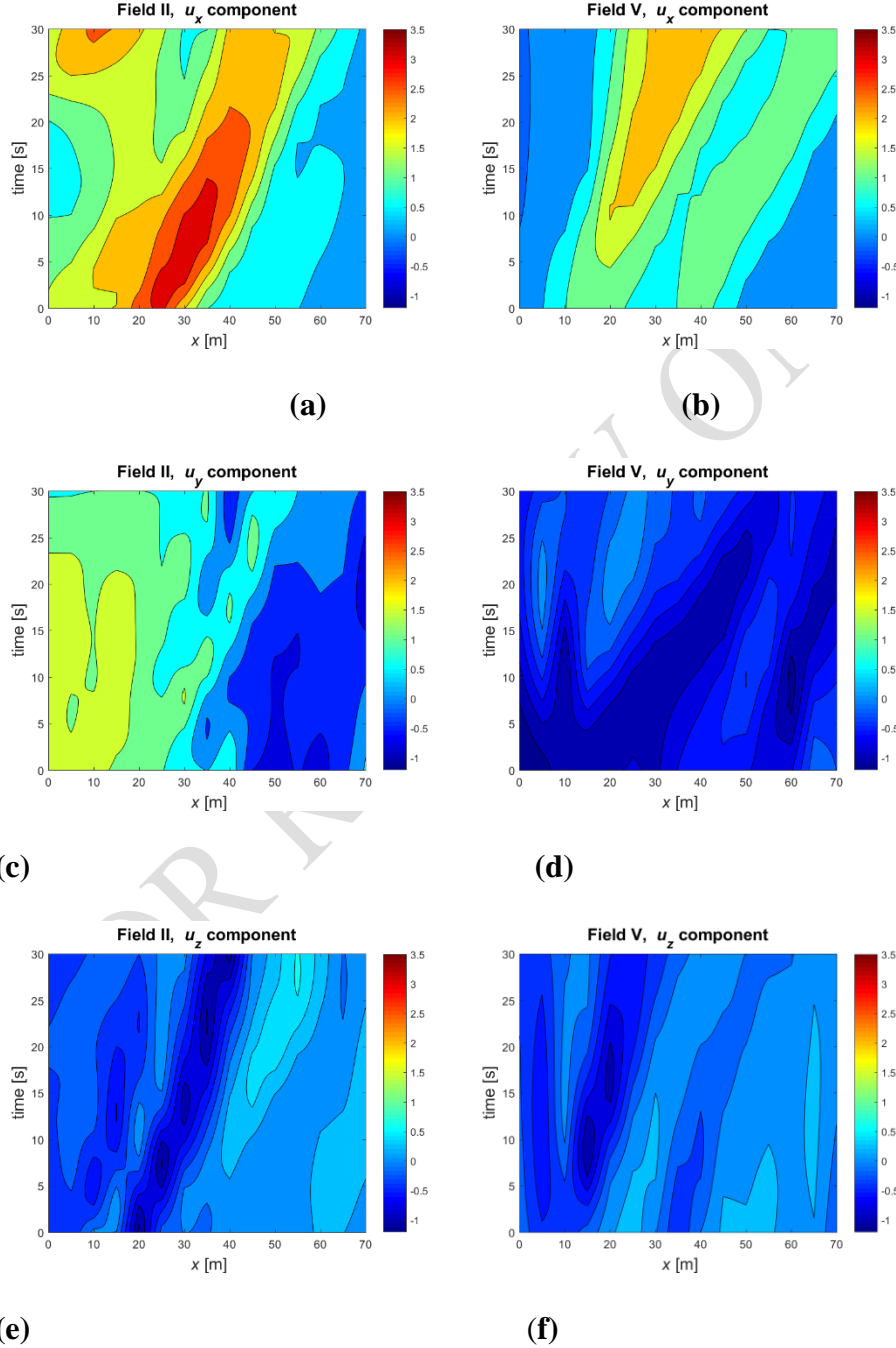36 lead to an unexpected arrow's trajectory, affecting the final score.
37
38 *Initial Conditions*
39
40   The initial position of the arrow corresponds to the fixed place at which
41 the archer holds it before performing the shot, thus the position of the center of

1 mass is x_0=0, y_0=0 and z_0=1.5 m. The center of the target is located 70 m away
2 in the positive x direction and z_{tar}=1.3 m from the ground.
3   We consider Φ_0= 0 and the value of Θ_0 is adjusted so that under still wind
4 conditions, the arrow hits the center of the target. Θ_0 depends on the
5
6 **Figure 4.** *Time Evolution of the Wind Components u_x (**a,b**), u_y (**c,d**) and u_z (**e,f**)*
7   *for the Fields II and V.*

8
9
10   **(a)**   **(b)**
11

12
13
14 **(c)**   **(d)**
15

16
17
18 **(e)**   **(f)**
19 *Source*: Authors.
20

characteristics of the arrow, initial velocity V_0 and initial angular velocities $\omega_{\theta 0}$ and $\omega_{\phi 0}$., initial velocity V_0 and initial angular velocities $\omega_{\theta 0}$ and $\omega_{\phi 0}$. The initial velocities for both types of arrows are listed in Table 2. The magnitude of the initial angular velocities plays an important role to reduce the angle of attack and the drag exerted on the arrow, as shown by Ortiz et al. [Ortiz et al., 2019]. Therefore, two different initial angular velocities are considered in a separated way. In the former, the angular velocities are assumed to be zero or $(d\boldsymbol{n}/dt)_0=0$, implying that

$$\omega_{\phi 0}= \omega_{\theta 0}=0, \tag{10}$$

$$\phi_0=0, \tag{11}$$

$$\theta_0=\Theta_0. \tag{12}$$

The second category is the so-called ideal initial angular velocity, defined as $(d\boldsymbol{n}/dt)_0=(d\boldsymbol{t}/dt)_0$. When the ideal initial angular velocity is achieved, the arrow almost aligns with $\boldsymbol{V}$-$\boldsymbol{U}$ and γ remains small enough to preserve the boundary layer laminar [Miyazaki et al., 2017]. For these kind of computations, the laminar value of C_D is used. When the zero initial angular velocity is considered, the turbulent value of C_D is introduced.

Results

In this section, the results obtained from the numerical computations are presented. In the first subsection the effects of uniform side-, head- and tail-winds in the trajectory are compared. Additionally, the influence of increasing the initial velocity of the arrows under side-winds is described.

Further, the role that the arrows' mass play in their behavior under velocity-changing wind fields is studied in detail. Finally, the trajectories of arrows for which the boundary layer transition, from laminar to turbulent regimes, takes place during the flight are compared.

Behavior of the Arrow Subject to a Uniform Background Wind.

As a first approach it is considered the influence of uniform winds. In these cases, the arrows are subject to the same wind velocity regardless their position. The three studied cases are the side-, head- and tail-winds. The side-wind (u_y) is exerted along the y-axis, whereas in the tail- ($u_x>0$) and head-winds ($u_x<0$), the air flow is in and against the x-direction, respectively. A wind velocity of 3 ms^{-1} is considered for all the uniform cases.

For the lighter type-A arrow, the time evolution of the angle of attack, γ, is shown in Fig.5 for the cases with zero initial angular velocity in the main area. The cases with ideal initial angular velocity are represented in the inserted

1 panel in the inferior part of the figure, whereas the panel in the right superior
2 part depicts the target and the points at which the arrows strike on it.
3   Miyazaki et al. [Miyazaki et al., 2017] proposed that the state of the
4 boundary layer might be inferred from the angle of attack, γ. For small angles
5 of attack, $\gamma<0.4°$, the boundary layer can be considered laminar, whereas for
6 $\gamma>0.6°$ the boundary layer appeared to be turbulent in most of the extension of
7 a type-A arrow. Therefore, the concept of a threshold value of the angle of
8 attack, γ_{thr}, can be introduced. If such γ_{thr} value is exceeded, the transition from
9 laminar to turbulent boundary layer would take place.
10   For the side-wind with zero initial angular velocity (—), an initial angle of
11 attack of $\gamma=3°$ might be large enough to provoke a turbulent boundary layer
12
13 **Figure 5.** *Main Area: Time Evolution of the Angle of Attack Considering Side-,*
14 *Head- and Tail-Winds with a Velocity of 3ms⁻¹ for the Cases with Zero Initial*
15 *Angular Velocity and Type-A Arrow. Inferior Panel: Cases with Ideal Initial*
16 *Angular Velocity. Inserted Panel in the Right: Striking Point in the Target for*
17 *all the Cases.*
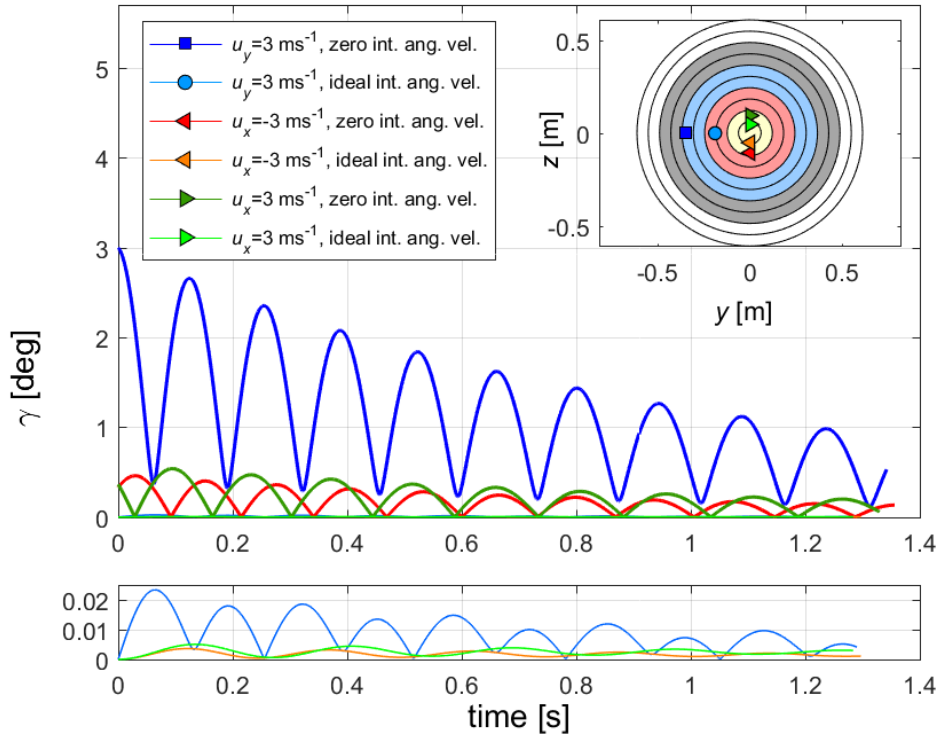
18
19 *Source*: Authors.
20
21   along the whole trajectory of the arrow, resulting in a final deviation from
22 the center of the target of around $\delta r=0.35$ m (■).
23   Due to the purely side-wind effect, the arrow shows only a lateral
24 deviation or wind drift. For the cases of tail- (—) and head-winds (—) with zero
25 initial angular velocity, the final deviations from the center of the target are
26 around $\delta r=0.10$ m (▶) and $\delta r=0.11$ m (◀), respectively. Which implies that

the side-wind affects in a more important way the trajectory of arrows in free-flight.

Consider the cases for which the ideal initial angular velocity is set in the computations, inserted panel in the inferior part of Fig.5, now the arrow almost aligns with the wind component and an angle attack close to zero is developed. The value of γ remains small enough to keep a laminar boundary layer and the deviation from the center of the target reduces to around δr=0.19 m ($\bullet$) for the side-wind. By keeping the arrow aligned with the wind flow and therefore the boundary layer laminar, it is possible to reduce the lateral deviation in the trajectory. Nevertheless, shooting the arrow with the ideal initial conditions might be challenging for the archers. Recently, Miyazaki et al. [Miyazaki et al., 2017] reported their experience in trying to adjust and control the arrows' initial angular velocity with little success.

In the Fig.6 it is shown that by increasing the arrow's initial velocity, V_0, it is possible to reduce the lateral deviation in the trajectory. Zero initial angular .

Figure 6. *Dependence of the Lateral Deviation in the Trajectory on the Initial Arrow's Velocity. Not Ideal Initial Angular Velocity and a Side-Wind of 3ms^{-1} were Considered*
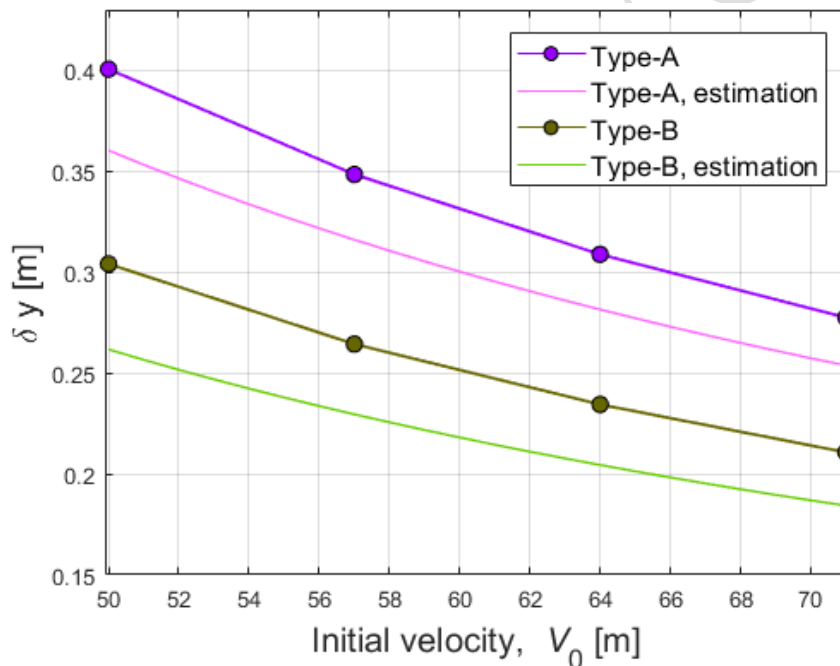
Source: Authors.

velocity and a uniform side-wind of 3 ms^{-1} was considered in the computations (— and —). If the typical velocity (V_0=57 ms^{-1}) for arrows shot with recurve bows is increased ~25%, a reduction in the lateral deviation of ~0.05 m and ~0.07 m can be expected for the heavier arrow and the lighter one, respectively. Arrows shot with compound bows generally have larger initial velocities, V_0>80 ms^{-1}, resulting in less deviated trajectories than those shot with recurve bows [Park, 2011]. Considering that the lateral deviation in the

trajectory or wind drift is mainly provoked by the lateral component of the
drag, a rough estimation of the wind drift can be approximated by

$$\delta y \sim \frac{F_D}{2M} \frac{u_y}{\sqrt{V_0^2 + u_y^2}} \left(\frac{L}{V_0}\right)^2 \sim \frac{c_D \rho \pi r^2}{4M} \frac{u_y}{V_0} L^2, \tag{13}$$

where F_D is the drag force and L is the length of the archery range. In Fig.
6 the results from the estimation (— and —) are plotted along with the results
from the numerical computations for both types of arrows. The difference from
the estimation and the numerical results arises from the assumption that in Eq.
(13) the velocity V_0 remains constant along the whole arrow's trajectory.
Whereas in an actual shot, the arrow's velocity was confirmed to reduce ~15%
and ~12% for the type-A and type-B, respectively.

Figure 7. *Computed Trajectories in all the Fields Using Different Starting Times. not Ideal Initial Angular Velocity was Considered in all the Cases for (**A**) Type-A And (**B**) Type-B Arrows.*
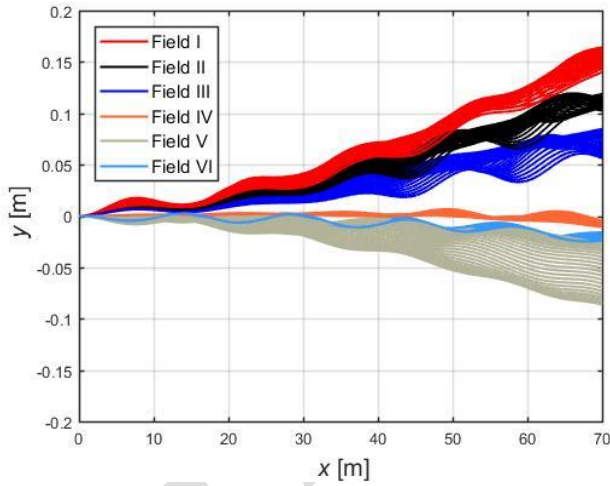

(a)
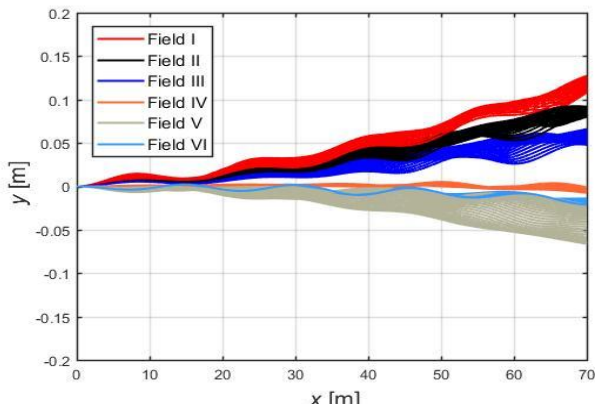
(b)

Source: Authors.

Influence of the Mass in a Changing Wind Field

Fig.7 shows an upper view of the computed trajectories for the type-A (Fig.7a) and type-B (Fig.7b) arrows with zero initial angular velocity. With multiple colors are represented the trajectories corresponding to the 6 different archery ranges. Multiple lines are plotted for different starting times with a delay of 1 s between them. By changing the starting time of the shot, it is possible to make sure that the arrows are subject to different wind fields during free-flight. Regardless of the location and wind behavior, the arrows with larger mass show less deviated trajectories (Fig.7b) than the lighter ones (Fig.7a). The lateral deviation in the trajectory decreases with increasing arrow's mass.

Figure 8. *Variation of the Wind Velocity with the Position Experienced by the type-A Arrows Showing Maximum and Minimum Values of δy in fields I (**a**) and III (**b**).*

(a)

(b)
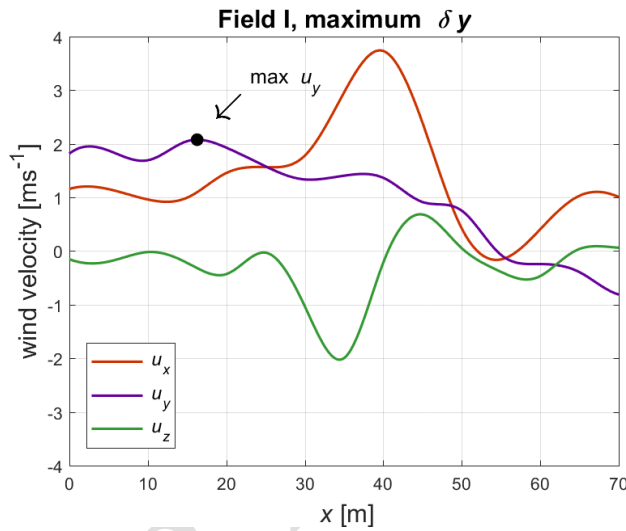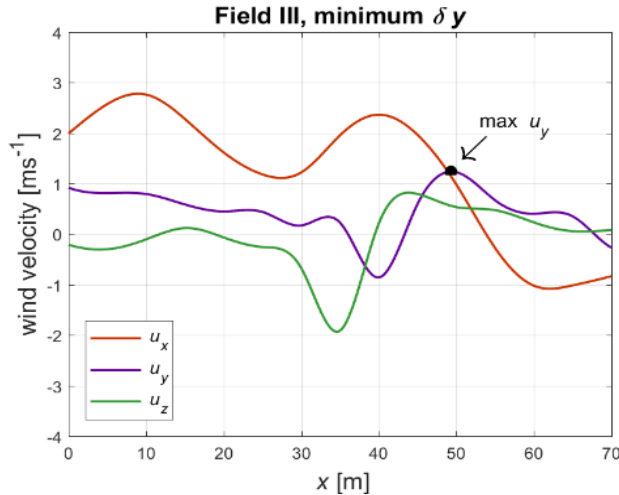
The averaged δy for each of the fields also change significantly, showing the different wind behavior for each of the locations. In the final round area (fields I, II and III), positive side-winds are exerted on the arrows, resulting in positive values of δy. Whereas for the ranking round area (fields IV, V and VI) the negative deviations were found as a result of the negative side-winds ($u_y<0$). The average and standard deviation of δy also varies from field to field. The averaged values of δy resulted in 0.15 m, 0.11 m and 0.07 m for the fields I, II and III respectively for the lighter arrow (Fig.7a). Appreciably larger values of the standard deviation in δy are present for the field V (—) compared with those of the field VI (—).

From the multiple shots with the type-A arrow and zero initial angular velocity were selected two cases in the final round area corresponding to the maximum and minimum δy, found in the fields I (—) and III (—), respectively. A difference in the lateral deviation of ~ 0.10 m between such cases is not negligible and may affect in an important way the final score in the competition.
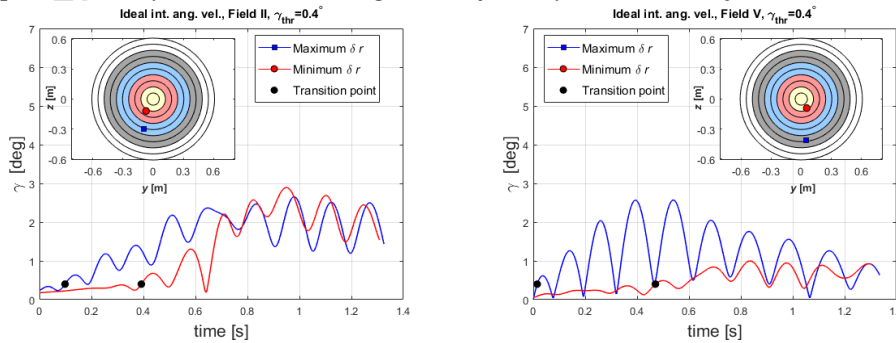
The wind velocity components, u_x, u_y and u_z, experienced by the arrows in those two cases is plotted in Fig.8. As the arrows fly in the archery range, the wind strength changes with position. In the case of maximum δy in the field I (Fig.8a), the maximum value of the side-wind u_y is 2.07 ms^{-1}. This side-wind velocity is exerted on the arrow for just a fraction of a second, in contrast to the cases of uniform side-wind, where the arrow experienced the same wind velocity along all the trajectory. For the case with minimum δy in the field III (Fig.8b), the maximum side-wind velocity experienced by the arrow is 1.23 ms^{-1}, from which the smaller δy arises. The influence of the side-wind is emphasized because it appears to be more dangerous for the shots than the head- and tail-winds, as shown in the inserted panel in Fig.5.

1

Vertical Drop of Arrows Shot with the Ideal Initial Angular Velocity

3

4 The Fig.9 shows the time evolution of the angle of attack, γ, for a type-A
5 arrow with the ideal initial angular velocities in the fields II and V with
6 γ_{thr}=0.4°. This implies that the boundary layer is initially laminar and becomes
7 turbulent once γ_{thr} is exceeded. There were performed computations for
8 multiple starting times with a time difference of 1 s between them. In the figure
9 are shown the shots with maximum (— and ■) and minimum (— and ●) values
10 of δr for each field. It is indicated with ● when the transition to turbulent
11 boundary layer takes place. For the field II in Fig.9a with maximum δr (■), the
12 transition to turbulent boundary occurs at ~0.1 s from the shot, leading to a
13 final radial deviation from the center of the target of δr=0.31 m. For the case of
14 minimum radial deviation (●), δr=0.14 m, with a retarded transition to
15 turbulent boundary layer, an improvement of more than 0.15 m could be
16 achieved. In Fig.9b for the field V, it is shown that delaying ~0.44 s the
17 transition to turbulent boundary layer may result in a significant reduction in
18 the radial deviation from the center of the target. The obtained values are
19 δr=0.41 m and δr=0.11 m for the earlier and the retarded transitions,
20 respectively. Moreover, for the case with minimum δr, the value of the angle of
21 attack remains small, $\gamma<1°$, during all the flight (—), thus generating small drag
22 and a less deviated trajectory.
23 In the Figs.9c-9f the wind components experienced by the arrows with
24 maximum and minimum values of δr are shown. An earlier transition to
25 turbulent boundary layer provokes that the arrows stay longer in the air,
26 because of the larger drag force, thus contributing to the vertical drop in the
27 trajectories. Further, in contrast to the cases with purely side-, head- and tail-
28 winds, the non-zero vertical wind component u_z (—) also induces deviation in
29 the z direction.

30

31 **Figure 9.** *Results for the Computations with Maximum and Minimum Values of*
32 *δr Considering a Threshold Angle of Attack γ_{thr}=0.4° for the Fields I and V*
33 *Using a type-A Arrow and Ideal Initial Angular Velocities. (a) and (b) Show*
34 *the time Evolution of the Angle of Attack, γ. Inserted Panels: Impact Points on*
35 *the Targets. Time Evolution of the Wind Components (u_x, u_y and u_z)*
36 *Experienced by the Arrow Along its Trajectory (c, d, e and f).*

37
38

1   **(a)**   **(b)**

2

3

4

5   **(c)**   **(d)**

6

7

8

9   **(e)**   **(f)**

10 *Source*: Authors.

11

12 **Figure 10.** *Results for the Computations for a type-A Arrow in the Field II*
13 *Using two Different Threshold Values of the Angle of Attack (γ_{thr}=0.4° and*
14 *γ_{thr}=0.6° With Ideal Initial Angular Velocity) and Fully Turbulent Boundary*
15 *Layer.*

16
17 *Source*: Authors.

18
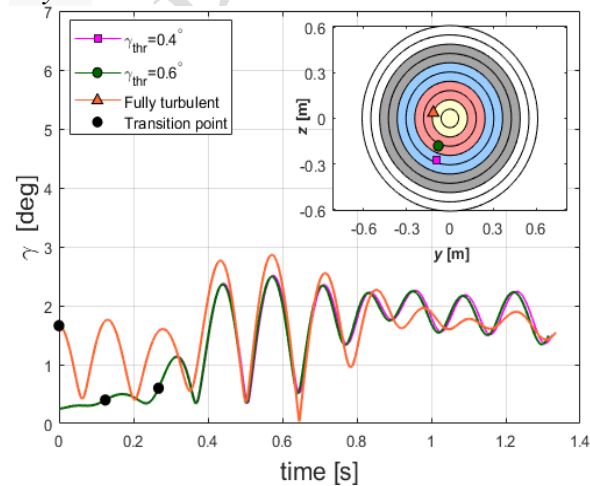
Discussion

It has been proposed that the transition to turbulent boundary layer may take place when the maximum angle of attack is located in the range $0.4° <\gamma_{max} < 0.6°$ for $Re=1.75\times10^4$ [Miyazaki, 2017]. As Re increases, the threshold angle at which the transition takes place decreases. Within the mentioned range, it is expected that exists a threshold angle, γ_{thr}, at which the transition occurs.

In this section, the influence of the value of such γ_{thr} is explored. Therefore, there were performed simulations considering transition to turbulent boundary layer with two different threshold values, $\gamma_{thr}=0.4°$ and $\gamma_{thr}=0.6°$, and compared with the case of a fully turbulent boundary layer. Fig.10 shows the time evolution of the angle of attack and in the inserted panel the target with the impact points on it. The ideal initial angular velocity was set for the cases with laminar-turbulent transition. On the other hand, a zero initial angular velocity was fixed in the fully turbulent computations. The characteristics of the type-A arrow were considered and the archery range where the shots were computed is the field II. For the case when $\gamma_{thr}= 0.4°$ was set (— and ■), a turbulent boundary layer is developed at ~0.12 s and results in a final deviation from the center of the target of $\delta r=0.29$ m.

On the other hand, when the threshold value was increased to $\gamma_{thr}= 0.6°$ (— and ●), the transition to turbulent boundary layer (●) took place at ~0.27 s after the shot was performed. For the latter case, the final deviation from the center of the target resulted in $\delta r=0.20$ m. Even though for both shots the boundary layer remains turbulent for most of the trajectory, a delay of ~0.15 s in the transition resulted enough to reduce ~0.09 m the radial deviation from the center of the target. Such reduction of the deviation in the trajectory might not be negligible to sum points in the final score. By keeping the boundary layer laminar the drag is reduced and therefore the deviation in the trajectory.

Consider now the case when the archer assumes zero initial angular velocity, i.e. not ideal initial conditions or turbulent boundary layer along the whole trajectory. In this case, the initial angle of attack presents a large enough value to generate a turbulent boundary layer from the beginning, $\gamma>1.6°$, nevertheless the radial deviation from the center of the target is $\delta r=0.12$ m. Even larger drag force might be exerted due to the magnitude of γ, the final deviation resulted smaller than the cases with transition during the flight. The final outcome appears to depend not only in the initial conditions, but also on the background wind characteristics. Even the archer was able to shoot the arrow with the ideal initial conditions, an unexpected wind behavior along the flight resulted in large trajectory deviations.

Conclusions

In this paper, we investigated the influence of background winds on archery arrows using a mathematical model. The archery competitions are

1 performed outdoors, therefore the background wind must be taken into because
2 it represents one of the most important elements disturbing the shots.
3   We assumed the arrows to behave as rigid bodies. By computing their
4 attitude, it was possible to obtain the time evolution of the angle of attack, from
5 which the state of the boundary layer was inferred.
6   In our simulations, we introduced the background wind information that
7 corresponds to the ground where the archery competitions will be held in the
8 Olympic Games of Tokyo in 2020. Such wind information provided by
9 JAMSTEC was the result of high-resolution large eddy simulations.
10   It was found that uniform side-wind disturbs more seriously the trajectory
11 of arrows than the uniquely head- and tail-winds. Nevertheless, in an actual
12 wind field the direction and wind velocity change with the location and time,
13 resulting in unexpected arrows' behavior.
14   Under a theoretical uniform side-wind, it appears feasible to keep the
15 boundary layer laminar along the complete trajectory by aligning the arrows'
16 attitude with the wind flow. By doing so, it is possible to reduce the wind drift.
17   The arrows' initial velocity and mass play a determinant role in the final
18 deviation from the center of the target. With increasing initial velocity and
19 mass, the arrows showed less deviated trajectories, regardless of the wind
20 behavior.
21   It was found that by delaying the transition from laminar to turbulent
22 boundary layer, deviations in the trajectory were reduced under certain
23 circumstances. The control of such transition has to be seriously considered.
24 Further, an unexpected behavior of the wind during the arrows' flight may
25 result in large deviations in their trajectory, even if the ideal initial conditions
26 are achieved. Under non-uniform velocity wind fields, trying to keep the
27 arrow's boundary layer laminar may be more harmful than beneficial.

References

Allen T and Goff J, 2017. Resources for sports engineering education, Sports Eng, 1-9
Goff J, 2013. A review of recent research into aerodynamics of sports projectiles, Sports Eng, 16, 137-154
Haake S, 2009. The impact of technology on sporting performance in Olympic Sports, J Sport Sci 27:13 1421-1431
Hubbard M, 1984. Simulation of javelin flight using experimental aerodynamic data, J Biomechanics 17:10, 769-776
Hubbard M, 1984. Optimal javelin trajectories, J Biomechanics 17:10, 777-787
Kooi B, 1998. Bow-arrow interaction in archery, J Sport Sci 16, 721-731
Matsuda, K., Onishi, R., and Takahashi K, 2018. Tree-crown-resolving large-eddy simulation coupled with three-dimensional radiative transfer model. J Wind Eng Ind Aerod 173, 53-66
Miyazaki T, Matsumoto T, Ando R, Ortiz J, Sugiura H, 2017. Indeterminacy of drag exerted on an arrow in free flight: arrow attitude and laminar-turbulent transition. Europhysics 38:6
Miyazaki T, Mukaiyama K, Komori Y, Okawa K, Taguchi S, Sugiura H, 2013. Aerodynamic properties of an archery arrow. Sports Eng 16 (1): 43-54

1 Ortiz J, Ando M, Murayama K, Miyazaki T, Sugiura H, 2019. Computation of the
2   trajectory and attitude of arrows subject to background wind. Sports Eng 22:7.
3   DOI=http://doi.org/10.1007/s12283-019-0302-9
4 Neda Y, Rajat M, 2018. A computational approach for predicting plant canopy
5   induced wind effects on the trajectory of golf shots. Sports Eng 21:1-10
6 Park J. Minimizing wind drift of an arrow, 2011. Proc Inst Mech Eng P J Sports Eng
7   Technol 226:52-60.
8 Park J, 2019. The impact of the atmosphere on target archery. Proc Inst Mech Eng P J
9   Sports Eng Technol. DOI=https://doi.org/10.1177/1754337118823967